Supporting Information

Eswaran et al. 10.1073/pnas.0901989106

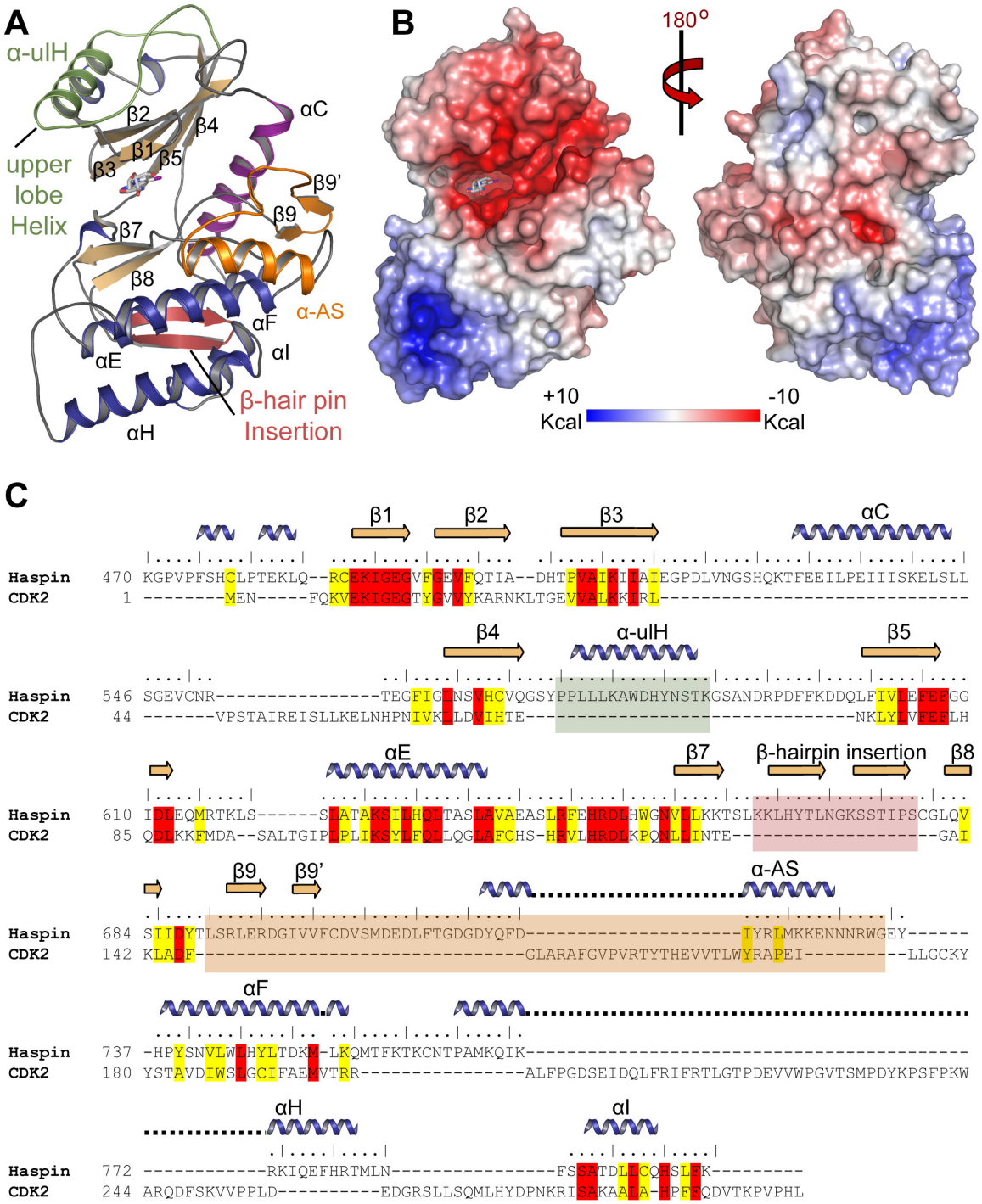

Fig. S1. Haspin surface electrostatics and structure-based alignment with CDK2 (PDB code 2UZO). Main secondary structure elements are shown in panel (*A*). Surface electrostatics reveal a negatively charged upper lobe that might serve as a docking site for histone H3 (*B*). The lower lobe contains a highly positively charged region. The main secondary structure elements are highlighted in the structure-based alignment in panel (*C*). Conserved residues are in red.

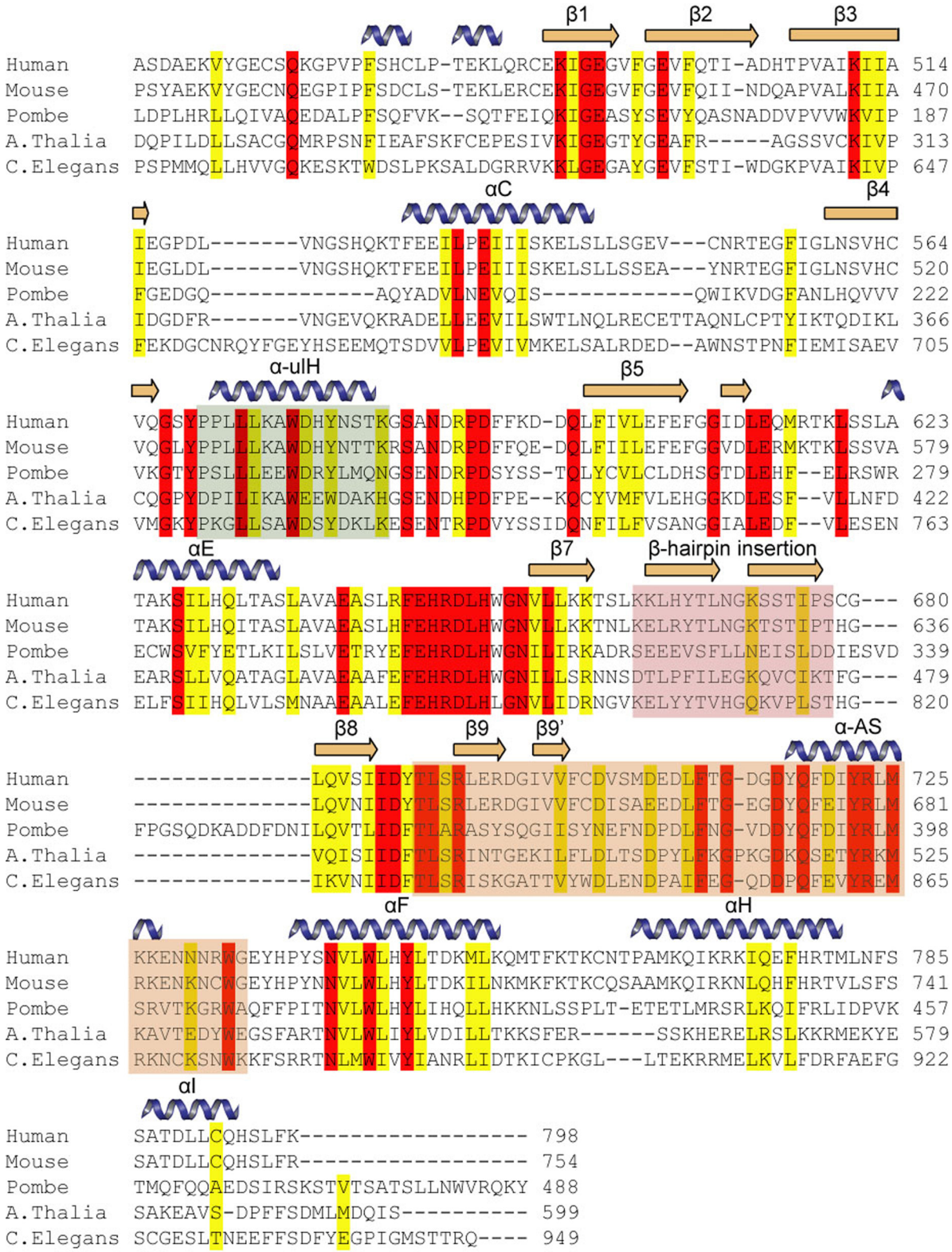

Fig. S2. Alignment of the kinase domains of haspin orthologues. The following sequences were used: human (gi56790919, NP_114171.2), mouse (gi7106329 NP_034483.1), *Schizosaccharomyces pombe* (gi19114088, NP_593176.1), *Actinote thalia* (gi 30681147, NP_172416.2), and *Caenorhabditis elegans* (gi212632867, NP_492043.2). Secondary structure elements and haspin specific inserts are highlighted.

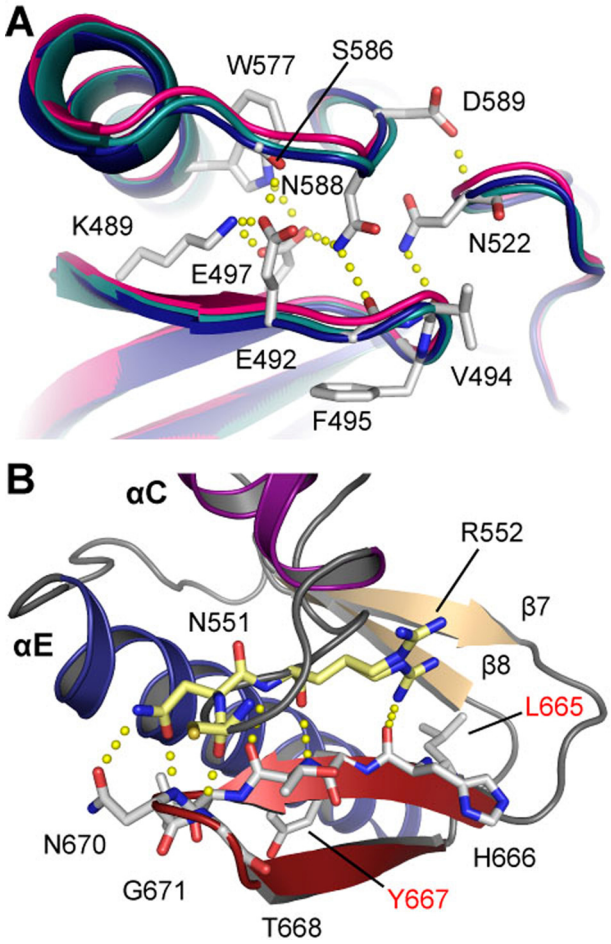

Fig. S3. Detailed view of the interaction of the ulH insert with the P-loop (*A*) and of the beta-hairpin insert with the loop C-terminal to helix αC (*B*). Hydrogen bonds are shown as dotted lines, and residues forming interactions are shown in stick representation and are labeled.

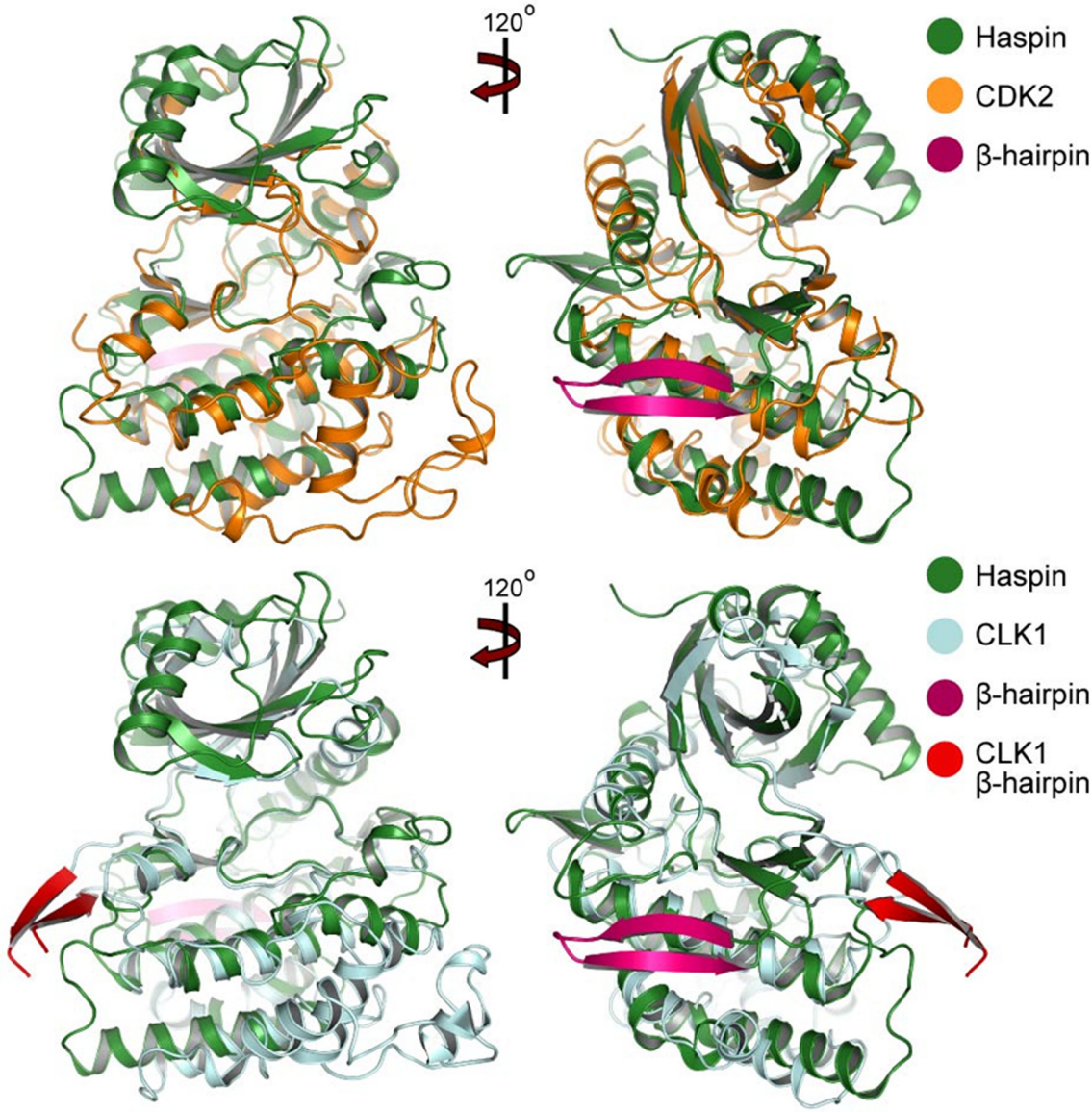

Fig. S4. Superimposition of haspin with CDK2 (PDB code 2UZO) (*Upper*) and CLK1 (PDB code 1Z57) (*Lower*). The structures superimposed with haspin with an rmsd of 1.92Å for 155 residues (CDK2) and 1.84Å for 181 residues (CLK1). Shown are ribbon diagrams. The β-hairpin insert present in the lower lobe is highlighted. In addition, CLK family members contain a β-hairpin insert at that position; however, this insert is oriented in a different way and makes no contact with the upper lobe.

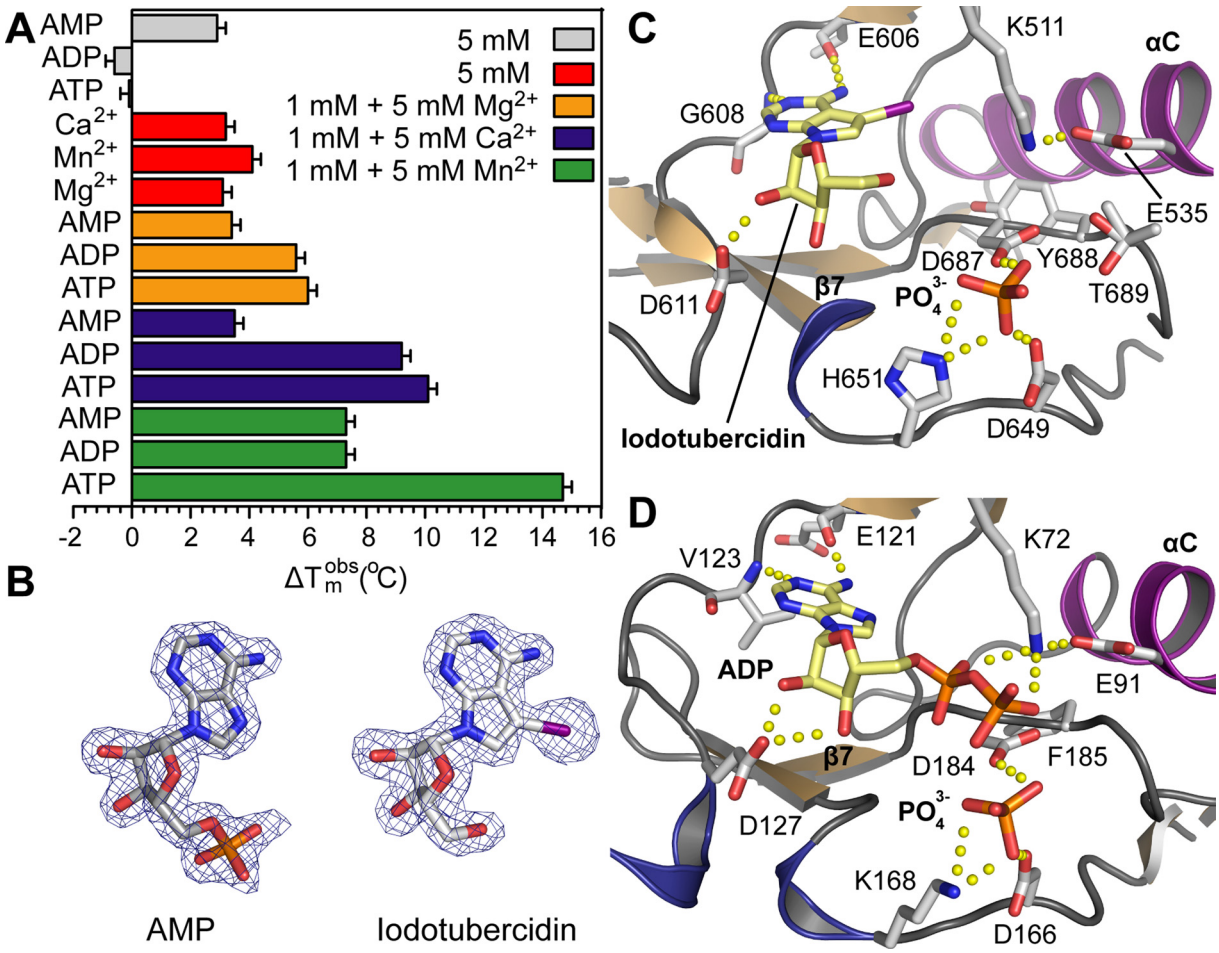

Fig. S5. Temperature shift data giving an estimate of the binding strength of nucleotides in the presence and absence of divalent ions. (*A*) Observed ΔTm values for divalent ions and nucleotides. The nucleotide concentration was 1 mM or 5mM, and the ion concentration was 5 mM. No significant ΔTm shift except for AMP was observed for nucleotides alone. The presence of divalent ions led to a stability increase of ≈3° (red). Combinations of both ions and nucleotides led to a significant ΔTm in the order ATP>ADP>AMP and Mn^{2+}>Ca^{2+}>Mg^{2+}. (*B*) AMP and iodotubercidin were well defined by electron density as shown in the $2F_oF_c$ electron density map contoured at 2σ. (*C*) Binding of iodotubercidin and a phosphate ion to the ATP site of haspin. The phosphate moiety mimics interactions of the γ-phosphate in ATP. (*D*) Binding of ADP and phosphate to PKA (PDB code 1RDQ) (*J Mol Biol* 2004;336:473–487). The comparison revealed that haspin H651 functionally replaces PKA K168 in forming hydrogen bonds with the γ-phosphate.

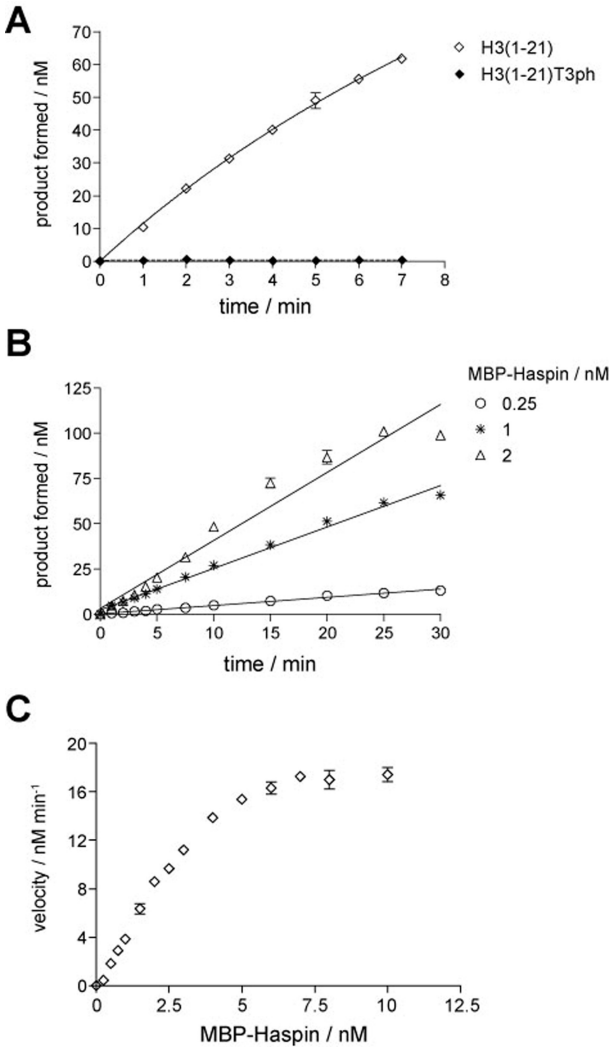

Fig. S6. Establishment of initial velocity conditions for MBP-haspin. (*A*) One μM H3 (1–21) or H3(1–21) T3ph peptides were tested as substrates in reactions ontaining 120 μM ATP and 6 nM MBP-Haspin. No phosphorylation was observed when H3(1–21) T3ph peptide, which represents the product of kinase reaction, was used. (*B*) Time course of phosphorylation of 0.8 μM H3 (1–21) peptide by various concentrations of MBP-haspin with 250 μM ATP. (*C*) Phosphorylation of 0.8 μM H3 (1–21) peptide as a function of MBP-haspin concentration (5-min reaction with 250 μM ATP).

A

Rank	Equation	R^2	AICc	Sy.x
1	Random Bi-Bi (Sequential)	0.974	-268.5	0.375
2	Ping-Pong Bi-Bi (Nonsequential)	0.970	-250.3	0.401
3	Ordered Bi-Bi (Sequential)	0.947	-173.4	0.528

B

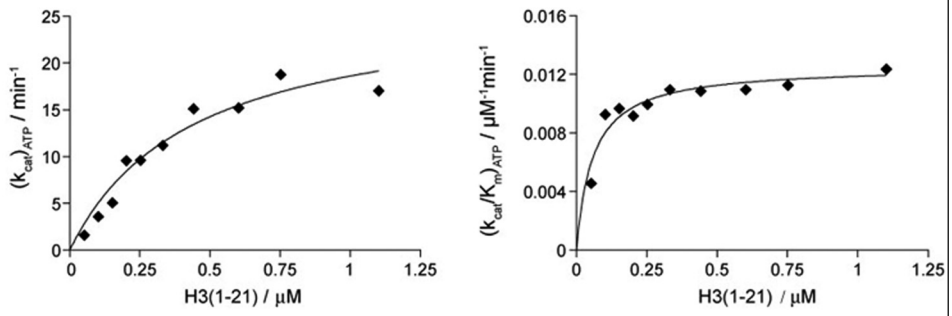

C

Product	Varied Substrate	Fixed Substrate	Inhibition type	K_i / μM
H3(1-21)T3ph	ATP	H3(1-21)	Non-competitive	0.51
H3(1-21)T3ph	H3(1-21)	ATP	Competitive	0.36
ADP	ATP	H3(1-21)	Competitive	420
ADP	H3(1-21)	ATP	Non-competitive	170

D

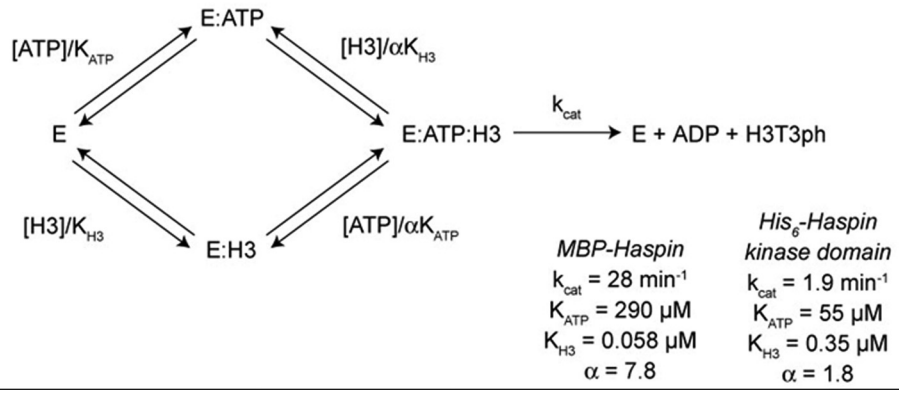

Fig. S7. Reaction mechanism of haspin. (*A*) Using nonlinear regression, the fit of the data in Fig. 4*B* to 3 kinetic mechanisms was ranked statistically by the coefficient of determination (R^2), the Akaike information criterion (AICc), and the standard deviation of residuals (Sy.x). All 3 provided support for a random mechanism. (*B*) The data in Fig. 4*B* were further analyzed by the method of replots (see text). Hyperbolic curves indicate a random sequential mechanism (also see Fig. 4 *C* and *D*). (*C*) Product inhibition studies with MBP-haspin were performed by determining initial reaction velocities in the presence of a fixed concentration of one substrate (near K_m concentration) as a function of concentration of the second substrate, at various fixed doses of product. Results were globally fitted to equations for competitive and noncompetitive inhibition and K_i (inhibition constant) were estimated using nonlinear regression analysis. (*D*) Summary scheme of the haspin reaction mechanism.

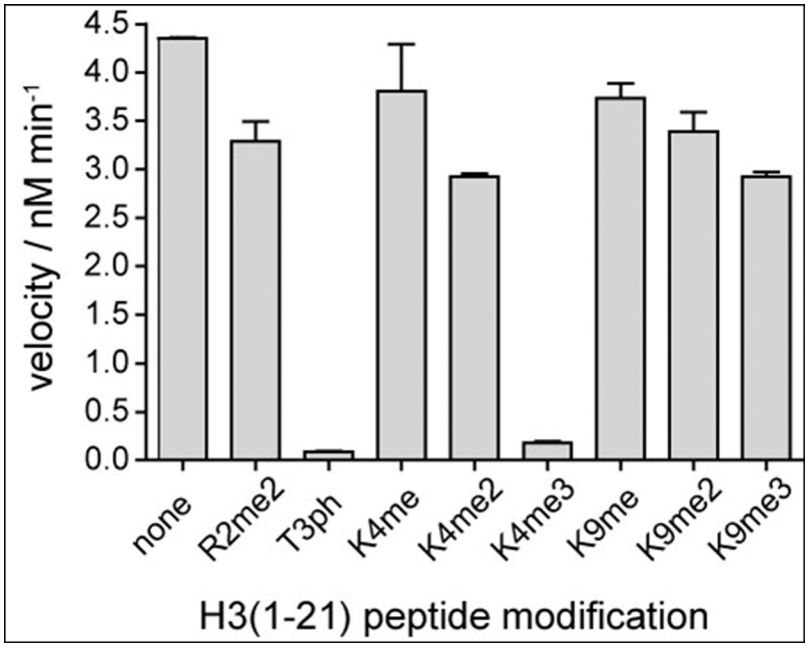

Fig. S8. Effect of histone H3 modifications surrounding Thr-3 on haspin activity. Kinase reactions were carried out with 6 nM His_6-haspin kinase domain, 1 μM H3 (1–21) peptide, and 120 μM ATP for 4 min.

Table S1. Data collection and refinement statistics

	Ligand		
	Iodotubercidin	AMP	Iodotubercidin/PO_4^{3-}
Data collection			
PDB code	2VUW	3DLZ	3IQ7
Space group	$P2_12_12_1$	$P2_12_12_1$	$P2_12_12_1$
Cell dimensions: a/b/c, Å	78.66/78.88/79.86	73.31/49.73/98.01	69.03/78.49/87.05
$\alpha/\beta/\gamma$, degrees	90.0/90.0/90.0	90.0/90.0/90.0	90.0/90.0/90.0
Resolution, Å*	1.80 (1.80–1.90)	1.85 (1.95–1.85)	2.00 (2.00–2.11)
Unique observations*	45,276 (5,506)	30,974 (4,362)	32,676 (4,697)
Completeness, %*	97.1 (82.9)	99.1 (97.6)	100.0 (100.0)
Redundancy*	3.5 (2.5)	2.9 (2.8)	3.6 (3.5)
Rmerge*	0.074 (0.358)	0.087 (0.512)	0.085 (0.620)
I/σI*	5.9 (2.2)	9.3 (2.0)	10.6 (2.0)
Refinement			
Resolution, Å	1.80	1.85	2.00
Rwork/Rfree, %	14.7/16.9	16.7/21.6	17.2/20.7
Number of atoms (protein/other/water)	2,941/22/411	2,669/32/462	2,641/35/262
B-factors (protein/other/water), $Å^2$	25.78/17.41/40.65	20.22/22.79/35.28	27.86/24.00/28.59
rmsd bonds, Å	0.010	0.016	0.016
rmsd angles, degrees	1.092	1.545	1.554
Ramachadran favored, %	96.37	96.63	95.95
Allowed, %	3.12	2.76	3.74
Disallowed, %	0.31	0.61	0.31

*Values in parentheses correspond to the highest-resolution shell.

Table S2. Comparison of kinetic parameters of full-length MBP-haspin and His_6-haspin kinase domain

	k_{cat} (min^{-1})	K_{H3} (μM)	K_{ATP} (μM)	α
MBP-haspin	28	0.058	290	7.8
His_6-kinase	1.9	0.35	55	1.8

Kinetic constants were estimated from nonlinear least squares fitting of replots (see Figs. 4 and S7), as described in ref. 19.